Environmental Science and Ecotechnology 25 (2025) 100567

Contents lists available at ScienceDirect

Environmental Science and Ecotechnology

journal homepage: www.journals.elsevier.com/environmental-science-and-ecotechnology/

Original Research

Chronic toxicity mechanisms of 6PPD and 6PPD-Quinone in zebrafish

Fang Jiao [a], Yang Zhao [b], Qiang Yue [c], Qi Wang [d], Zhongzhi Li [a], Wanjing Lin [a], Lingxi Han [e, *], Liangfu Wei [a, c, f, g, **]

[a] College of Marine Sciences, South China Agricultural University, Guangzhou, 510640, China
[b] Zhejiang Academy of Agricultural Sciences, Hangzhou, 310058, China
[c] Guangdong Provincial Key Laboratory of Utilization and Conservation of Food and Medicinal Resources in Northern Region, Shaoguan University, Shaoguan, 512005, China
[d] Key Laboratory of Drinking Water Science and Technology, Research Center for Eco-Environmental Sciences, Chinese Academy of Sciences, Beijing, 100085, China
[e] College of Horticulture, Qingdao Agricultural University, Qingdao, 266109, China
[f] Guangdong-Hong Kong Joint Laboratory for Water Security, Zhuhai, 519087, China
[g] Xiamen Key Laboratory of Intelligent Fishery, Xiamen, 361100, China

ARTICLE INFO

Article history:
Received 10 November 2024
Received in revised form
29 April 2025
Accepted 29 April 2025

Keywords:
6PPD
6PPDQ
Hepatotoxicity
PPARγ
zebrafish

ABSTRACT

N-(1,3-Dimethylbutyl)-N′-phenyl-p-phenylenediamine (6PPD) and its oxidation derivative, 6PPD-quinone (6PPDQ), have been extensively detected in environmental and biological samples, raising significant concerns regarding their chronic aquatic toxicity at environmentally relevant concentrations. However, the underlying mechanisms driving this chronic toxicity remain largely unexplored. Here we show that zebrafish exposed to 6PPD and 6PPDQ exhibit distinct toxicokinetic profiles, with 6PPD preferentially accumulating in the liver and 6PPDQ predominantly targeting the brain. Exposure to both compounds impaired zebrafish growth, induced hepatic damage, and disrupted locomotor behavior. Transcriptomic analysis of liver tissue revealed disturbances in lipid and carbohydrate metabolic pathways in both treatment groups, with distinct differences in gene expression patterns and biochemical responses between 6PPD and 6PPDQ. Specifically, both compounds downregulated peroxisome proliferator-activated receptor gamma (PPARγ) and elevated the expression of pro-inflammatory cytokines (TNF-α and IL-6). Molecular dynamics simulations and surface plasmon resonance experiments further demonstrated that hepatotoxicity was associated with direct binding of these compounds to PPARγ, a critical regulator of lipid metabolism and inflammation. Our findings highlight the hepatotoxic risks of 6PPD and 6PPDQ to aquatic life. Importantly, 6PPDQ exhibited greater toxicity compared to 6PPD, emphasizing an urgent need for targeted environmental controls and regulatory actions to mitigate ecological harm and potential public health consequences.

1. Introduction

N-(1,3-Dimethylbutyl)-N′-phenyl-p-phenylenediamine (6PPD) serves as a crucial antioxidant in rubber tires and protects various commercial rubber products—including vehicle tires, rubber pipes, and shoes—from the harmful effects of high temperatures, pressure, oxygen, and the ozone [1]. However, the extensive production and use of 6PPD has resulted in significant environmental contamination [2–4]. This issue is further compounded by the transformation of 6PPD in tire debris into 6PPD-quinone (6PPDQ) through thermal oxidation and photooxidation, particularly in aqueous environments where 6PPD is more easily converted to 6PPDQ [5]. Both 6PPD and 6PPDQ have been detected in aquatic environments worldwide [5–7]. The average concentrations of 6PPD and 6PPDQ in urban runoff water worldwide range from 0.21 to 2.71 μg L^{-1} for the former and 0.21–2.43 μg L^{-1} for the latter [3,8–10]. Additionally, these compounds have been found in various aquatic species, such as snakehead, weever, and Spanish

* Co-corresponding author.
** Corresponding author. College of Marine Sciences, South China Agricultural University, Guangzhou, 510640, China.
E-mail addresses: hanlingxi@qau.edu.cn (L. Han), liangfuwei@scau.edu.cn (L. Wei).

https://doi.org/10.1016/j.ese.2025.100567

mackerel [11,12]. The widespread presence of 6PPD and 6PPDQ in biological and environmental media emphasizes their potential risks to aquatic ecosystems and human health.

Recent research has elucidated the developmental, reproductive, and organ toxicities associated with 6PPD and 6PPDQ across non-target species, including humans, mice, zebrafish, and *Caenorhabditis elegans* (*C. elegans*). In *C. elegans*, exposure to 6PPDQ has been revealed to cause abnormal locomotor behavior and reduced lifespan at concentrations ranging from 0.1 to 10 μg L^{-1}, with neurodegeneration observed at 10 μg L^{-1} [13,14]. In zebrafish, exposure to 6PPD and 6PPDQ during early development (0–96 h post-fertilization) at concentrations of 10 and 25 μg L^{-1} was found to result in morphological changes, behavioral toxicity and cardiotoxicity in larvae [15,16]. Additionally, exposure of zebrafish embryos to 6PPD at 0.22 mg L^{-1} (2–120 h post-fertilization) was found to induce developmental toxicity and alterations in hormone levels and gene expression related to Growth Hormone/Insulin-like Growth Factor axis and Hypothalamic–Pituitary–Thyroid axis [17]. In male mice, sub-lethal exposure to 6PPDQ at 4 mg kg^{-1} was found to lead to significant reproductive deficits, which were characterized by diminished hormone levels and compromised semen quality [18]. Moreover, exposure to 6PPD and 6PPDQ at concentrations of 10–100 mg kg^{-1} was found to cause hepatotoxicity, as evidenced by dose-dependent liver bioaccumulation, increased liver weight, and elevated triglyceride levels in mice [19]. Furthermore, additional studies have linked environmental exposure to 6PPDQ at levels ranging from 1.3 to 30.3 ng g^{-1} to developmental delays in children [20].

Further, although recent studies have shed light on the toxicokinetics and tissue accumulation of 6PPDQ in adult zebrafish—including its specific accumulation in the brain, intestine, and eyes of zebrafish—significant gaps remain in understanding the bioaccumulation and toxicokinetics of 6PPD itself. Furthermore, the long-term chronic effects of both compounds on specific target organs, such as the liver, are poorly understood [21]. The mechanisms underlying internal exposure risks remain unclear, particularly in chronic exposure scenarios. Addressing these gaps is crucial to fully understand the toxicity of 6PPD and 6PPDQ in aquatic species.

Zebrafish are extensively utilized as a primary model organism for risk assessment and aquatic toxicology studies concerning hazardous chemicals, due to their ease of rearing, fully sequenced genome, and low cost [22,23]. In this study, we investigated the toxicokinetic characteristics of 6PPD and 6PPDQ in zebrafish tissues and examined the potential metabolic disruptions through multiple endpoints following exposure to environmentally relevant concentrations of these compounds. In addition, we integrated transcriptomic analysis, molecular dynamics simulations, and surface plasmon resonance (SPR) to explore the hepatotoxic mechanisms of these compounds. This multimethod approach enabled us to uncover molecular interactions, gene expression changes, and protein-binding dynamics, thus providing a comprehensive understanding of the metabolic disruptions and chronic hepatotoxicity induced by 6PPD and 6PPDQ. By coupling these techniques, we provide a novel framework for assessing the long-term toxic effects of environmental contaminants in aquatic species.

2. Materials and methods

2.1. Chemicals and reagents

6PPD (Chemical abstracts service (CAS) No.: 793-24-8; purity ≥98%) and 6PPDQ (CAS No.: 2754428-18-5; purity ≥95%) were acquired from Cayman Chemical Co., Ltd (Ann Arbor, Michigan, USA). Dimethyl sulfoxide (DMSO), Tricaine methanesulfonate (MS-222), and GW9662 (CAS No.: 22978-25-2; ≥98%) were purchased from Sigma-Aldrich (St. Louis, MO, USA). Then, solutions of 6PPD and 6PPDQ were meticulously prepared at a standardized concentration of 8 mg L^{-1} and subsequently stored at −20 °C, intended for use within one month. Further, human peroxisome proliferator-activated receptor gamma (hPPARγ) protein was sourced from Cusabio (Wuhan, China). All chemicals and reagents used in this study were of analytical grade.

2.2. Zebrafish maintenance and experimental design

Male zebrafish of the wild-type AB strain, aged three months, were acquired from the China Zebrafish Resource Center (Wuhan, China). Upon arrival, they were acclimatized in aerated glass tanks (51 × 38 × 24 cm) at 26 ± 1 °C, with a 14:10 h light–dark cycle. Following acclimatization, zebrafish of similar sizes and weights were randomly divided into various experimental groups. In the toxicokinetic study, zebrafish were exposed to 0 or 8 μg L^{-1} concentrations of 6PPD or 6PPDQ. Each tank, which served as an individual experimental unit, contained 40 male fish and was replicated thrice ($n = 3$) for each condition. Both vehicle control (VC) and treated groups received 0.001% (v/v) DMSO, with daily renewal of the exposure solution to ensure consistency. Since the exposure solutions were renewed daily, concentrations of 6PPD and 6PPDQ in the exposure solutions were determined only at 0 and 24 h. Ensuring we adhered to the pharmacokinetic experimental protocols (GB/T21750-2008), we measured the concentrations of 6PPD or 6PPDQ in the brain, liver, gonads, and muscle tissues of the zebrafish at specific intervals—on days 1, 4, 7, 14, 21, and 28—throughout the 28-day exposure. Subsequently, a 14-day non-exposure study was undertaken, during which tissue samples were collected on days 7 and 14 for further analysis.

In the toxicology experiment, another group of zebrafish was exposed to either 6PPD or 6PPDQ at concentrations of 0, 2, 4, and 8 μg L^{-1} (VC) for three months in 40-L glass tanks. This experiment involved 840 adult zebrafish, with 30 fish per treatment, distributed across four tanks each. The selected exposure concentrations were based on the reported environmental levels of these chemicals in aquatic ecosystems. The average concentrations in urban runoff worldwide range from 0.21 to 2.71 μg L^{-1} for 6PPD and 0.21–2.43 μg L^{-1} for 6PPDQ, with surface water concentrations reaching up to 0.91 μg L^{-1} [3,8,9]. Given these levels, our exposure concentrations represent environmentally relevant conditions, particularly in areas influenced by roadway runoff while also allowing for assessing the potential long-term toxic effects at higher concentrations. Additionally, the selected doses were informed by previous acute aquatic toxicity tests [24,25]. Following the three-month exposure period, we recorded survival and growth parameters, including weight and length. To ensure humane end-of-study procedures, the fish were anesthetized with MS-222 before dissection. Thereafter, we immediately harvested liver samples for various analyses and preserved them in liquid nitrogen for future assays. A subset of liver samples was fixed in 4% paraformaldehyde for histological examination, and serum was collected for biochemical assays. It must be noted that this study was conducted in strict compliance with the South China Agricultural University's ethical guidelines for the care and use of laboratory animals.

2.3. Chemical quantification in exposure solutions and zebrafish tissues

The actual concentrations of 6PPD and 6PPDQ in the exposure solutions ($n = 3$ replicates per treatment) and in the livers of the fish ($n = 3$ replicates) were determined using a slightly modified version of a previously published method [25]. Tissue samples from

10 individual fish were pooled to form a single replicate. The quantification of 6PPD and 6PPDQ was performed using liquid chromatography–tandem mass spectrometry (LC–MS/MS) (Waters, Massachusetts, USA). Comprehensive details on the extraction, clean-up, and analysis of 6PPD and 6PPDQ, as well as quality assurance and quality control procedures, are provided in Supplementary Material S1.1.

2.4. Physiological and biochemical analysis

Histological analysis of liver tissues from 10 fish per group ($n = 4$ replicates) was performed after fixation in 4% paraformaldehyde, dehydration, paraffin embedding, and sectioning into 5-μm slices. Hematoxylin and eosin (H&E) staining was conducted for examination, and Oil Red O staining was performed to confirm steatosis in frozen liver sections. Further, the biochemical parameters of plasma and liver tissues were assessed from pooled plasma of six fish per group ($n = 6$), with detailed assay protocols provided in Supplementary Materials S1 and S2. Further, the ecological risk of 6PPD and 6PPDQ to zebrafish was evaluated using the integrated biomarker response (IBR) analysis, as described in Beliaeff and Burgeot [26] and Guerlet et al. [27].

2.5. Transcriptome analysis and RT-qPCR validation

To investigate the mechanisms of hepatotoxicity induced by 6PPD and 6PPDQ in zebrafish, liver samples from both the VC and 8 μg L^{-1} 6PPD/6PPDQ exposure groups were collected for ribonucleic acid (RNA) sequencing on an Illumina HiSeq 6000 platform (California, USA), with detailed procedures provided in the Supplementary Material S1.3. Fifteen candidate genes were selected for quantitative polymerase chain reaction (RT-qPCR) using the primer pairs listed in Table S1 (Supplementary Material), and the RT-qPCR protocol is described in Supplementary Material S1.4 [28]. In addition, the mRNA levels of target genes were calculated and normalized against the housekeeping gene β-actin using the $2^{-\Delta\Delta CT}$ method [29].

2.6. Western blot analysis

Following the three-month exposure period, protein expression levels of PPARγ, TNF-α, and IL-6 in the liver were analyzed. Western blotting was performed according to established protocols [30], with detailed information provided in Supplementary Material S1.5.

2.7. Immunohistochemical localization

Immunofluorescence staining of zebrafish liver was performed following a published protocol [31]. After exposure, zebrafish were euthanized with 0.1% MS-222, and liver tissues (10 fish, $n = 4$ replicates) were dissected and sectioned into 5-μm slices using a paraffin microtome (HM355S, Thermo Scientific, Shanghai, China). Thereafter, the sections were deparaffinized and rehydrated through a graded alcohol series and xylene. Following rehydration, the sections were blocked with 5% bovine serum albumin (BSA) in phosphate-buffered saline (PBS) for 1 h at room temperature (RT). After the blocking step, the primary antibody was applied and incubated overnight, followed by incubation with the fluorescent secondary antibody for 2 h at RT. Then, the slides were rinsed with PBS, and the nuclei were stained with 4′,6-diamidino-2-phenylindole (DAPI, Sigma, St. Louis, MO, USA) for 30 min. Finally, the stained slides were examined using an Eclipse Ci-L fluorescence microscope (Nikon, NY, USA).

2.8. Simulation of molecular dynamics (MD) and binding kinetics

To evaluate the stability of the 6PPD-zebrafish PPARγ (zfPPARγ) and 6PPDQ-zfPPARγ complexes, molecular dynamics (MD) simulations were performed using GROMACS (version 2023.2) based on optimized molecular docking models. The detailed procedures for this are provided in Supplementary Material S1.6.

Further, the direct binding kinetics and affinity of 6PPD and 6PPDQ with hPPARγ were assessed using the Biacore™ T200 system (GE Healthcare, Madison, USA) through surface plasmon resonance (SPR) analysis. Recombinant PPARγ protein (Cusabio, Wuhan, China) was covalently immobilized onto a CM5 sensor chip (carboxymethylated dextran-coated chip, GE Healthcare, Sweden) using N-2-(hydroxyethyl)piperazine-N'-(2-ethanesulfonic acid) (HEPES) at pH 7.4. Various concentrations of 6PPD and 6PPDQ (5, 15, 45, 90, 180, 360, and 720 μM) were prepared in a HEPES buffer containing 1% DMSO at pH 7.4, which also served as the running buffer. All chemicals were injected at a flow rate of 30 μL min^{-1}. The association phase of the SPR measurement for each chemical lasted 60 s, followed by a dissociation phase that lasted 90 s.

2.9. Measurement of the locomotor activity in adult zebrafish

After a three-month exposure period, zebrafish were randomly selected for behavioral testing to mitigate potential bias. Measures were taken to minimize interference, such as noise, during recording. The locomotor activity of 16 zebrafish in each exposure group was evaluated using a video-track system (ViewPoint Life Science, Montreal, Canada). Each zebrafish was placed in an individual cylindrical container, measuring 9.4 cm in width and 14.1 cm in length. After a 10-min adaptation period, the swimming behavior of the fish was recorded for 5 min.

2.10. Statistical analysis

IBM SPSS Statistics 26.0 (IBM Corp., Armonk, NY) was used to analyze the experimental data. Kolmogorov–Smirnov and Levene's tests were employed for normality and variance homogeneity, respectively. Further, means ± standard deviation (SD) were calculated for each group. Group differences were assessed using a one-way analysis of variance (ANOVA), followed by Duncan's multiple-range test for post hoc analysis. Statistical significance was considered at $P < 0.05$, with $P < 0.01$ indicating high significance.

3. Results

3.1. Toxicokinetic parameters of 6PPD and 6PPDQ in zebrafish tissues

The concentrations of 6PPD and 6PPDQ in the exposure solution were analyzed and revealed fluctuations between 0 and 24 h. The degradation rates of 6PPD ranged from 0.75% to 3.06% (Supplementary Material Fig. S1a during the renewal interval, while those for 6PPDQ ranged from 0.38% to 1.01% (Supplementary Material Fig. S1b). These fluctuations in the exposure solution were deemed acceptable according to the guidelines of the Organization for Economic Cooperation and Development (1998) [32]. Additionally, in the VC group, the concentrations were below the detection limit (0.45 μg L^{-1}).

The concentrations of 6PPD and 6PPDQ were measured in the brain, liver, gonads, and muscle tissues of the zebrafish (Fig. 1). Both 6PPD and 6PPDQ levels were found to gradually increase during the first two weeks, with divergent accumulation patterns among different tissues and between the two chemicals in the days that

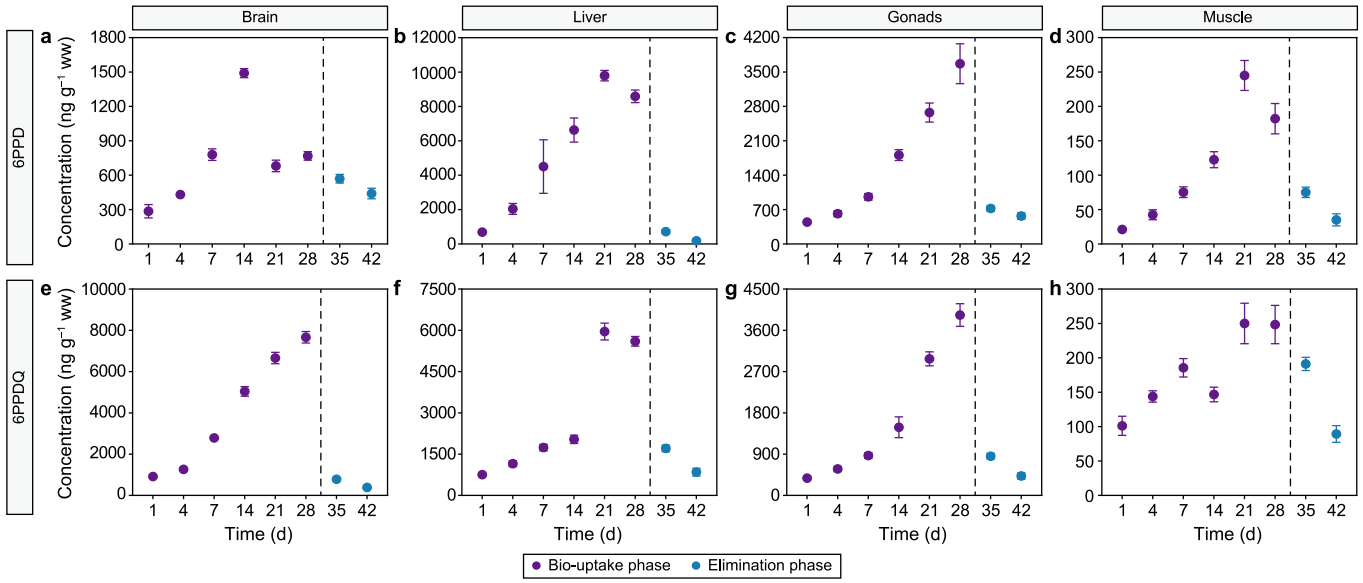

Fig. 1. Bioaccumulation and elimination kinetics of 6PPD (**a**–**d**) and 6PPDQ (**e**–**h**) in brain (**a**, **e**), liver (**b**, **f**), gonads (**c**, **g**), and muscle (**d**, **h**) tissues. Values are presented as mean ± standard deviation ($n = 3$).

followed. For 6PPD, concentrations peaked on days 14 and 21 in the brain, liver, and muscle tissues, and persisted in the gonads until day 28 (Fig. 1a–d). In the case of 6PPDQ, concentrations persisted in the brain and gonads until day 28, peaking in the liver and muscle tissues on day 21 (Fig. 1e–h). Throughout the 28-day enrichment period, the most significant accumulation of 6PPD was in the liver (9793.67 ± 303.84 ng g^{-1}), followed by that in the gonads (3668.89 ± 405.32 ng g^{-1}), brain (1490.56 ± 39.85 ng g^{-1}), and muscle tissues (244.96 ± 21.79 ng g^{-1}). Conversely, the highest accumulation of 6PPDQ was found in the brain (7664.02 ± 277.56 ng g^{-1}), followed by that in the liver (5957.29 ± 305.87 ng g^{-1}), gonads (3934.01 ± 247.21 ng g^{-1}), and muscle tissues (250.00 ± 29.39 ng g^{-1}) of the zebrafish. Specifically, the liver had the highest levels of 6PPD, and the brain showed the highest levels of 6PPDQ. Additionally, the peak concentration of 6PPDQ in the brain of the zebrafish was 5.14 times higher than the corresponding concentration of 6PPD, while that in the liver was 0.61 times lower than the corresponding concentration of 6PPD.

Further, the concentration data for 6PPD and 6PPDQ obtained during the bio-uptake and elimination phases were well-fitted using a classical pseudo-first-order toxicokinetic model. The kinetic bioconcentration factor (BCF_k) and uptake rate (K_{up}) were highest in the liver of the zebrafish in the 6PPD-exposure groups; in contrast, BCF_k and K_{up} were highest in the brain of the zebrafish in the 6PPDQ-exposure groups. The corresponding values for muscle tissues were the lowest for the zebrafish in both the 6PPD- and 6PPDQ-exposure groups (Supplementary Materials Tables S2 and S3).

3.2. Growth impairment and liver pathology induced by 6PPD and 6PPDQ in zebrafish

Exposure to 6PPD significantly reduced the body length of adult zebrafish in the 4 and 8 μg L^{-1} groups, while 6PPDQ exposure caused a significant decrease in body length across all exposure groups compared to the VC (Fig. 2a). In contrast, exposure to 6PPD significantly increased body weight in all groups, whereas exposure to 6PPDQ resulted in a significant weight increase only in the 4 and 8 μg L^{-1} groups (Fig. 2b). Additionally, exposure to 6PPDQ led to a significantly higher hepatosomatic index in all exposure groups, while significant changes in this index were observed only in the 8 μg L^{-1} 6PPD group (Fig. 2c).

Further, H&E staining revealed hepatic steatosis and mild ballooning degeneration in zebrafish exposed to 6PPD at 4 and 8 μg L^{-1}, while zebrafish exposed to 6PPDQ exhibited pronounced ballooning degeneration and pyknotic nuclei (Fig. 2d). Moreover, statistical analysis revealed a significant increase in the percentage of pathological phenotypes in the 4 and 8 μg L^{-1} groups compared to the VC group, with exposure to 6PPDQ causing a dose-dependent increase in these changes (Fig. 2e). Oil Red O staining confirmed lipid accumulation in groups of zebrafish exposed to both 6PPD and 6PPDQ, with moderate lipid staining in the 6PPD groups and a dose-dependent increase in lipid accumulation in the 6PPDQ groups (Fig. 2f). Consistent with these observations, the statistical analysis of Oil Red O staining revealed that exposure of zebrafish to 4 and 8 μg L^{-1} of 6PPD and 6PPDQ, respectively, significantly increased the lipid droplet content in the liver of the zebrafish (Fig. 2g).

3.3. Exposure to 6PPD and 6PPDQ affected liver function

To further evaluate chemical-induced hepatic toxicity, we measured hepatic toxicity biomarkers (Fig. 3). Alanine aminotransferase (ALT) activities were found to have increased significantly by 1.39- and 1.58-fold while aspartate aminotransferase (AST) activities rose by 1.48- and 1.79-fold in the 4 and 8 μg L^{-1} 6PPD-exposure groups compared to the VC group (Fig. 3a and b). In the 6PPDQ-exposure groups, ALT activities also significantly increased by 1.20-, 1.38-, and 1.72-fold across all exposure levels, while AST activities increased by 1.33- and 1.48-fold only at the higher concentrations of 4 and 8 μg L^{-1}, respectively (Fig. 3a and b). Similarly, alkaline phosphatase (ALP) activities significantly increased by 1.36- and 1.55-fold in the 4 and 8 μg L^{-1} 6PPD-exposure groups, respectively, and increased across all 6PPDQ-exposure groups by 1.27-, 1.59-, and 2.22-fold (Fig. 3c). In the 6PPD-exposure groups, superoxide dismutase (SOD) activities decreased significantly by 0.83- and 0.53-fold; moreover, glutathione peroxidase (GSH-Px) activities also decreased by 0.61-, 0.53-, and 0.46-fold, while malondialdehyde (MDA) content increased by 1.39- and 1.82-

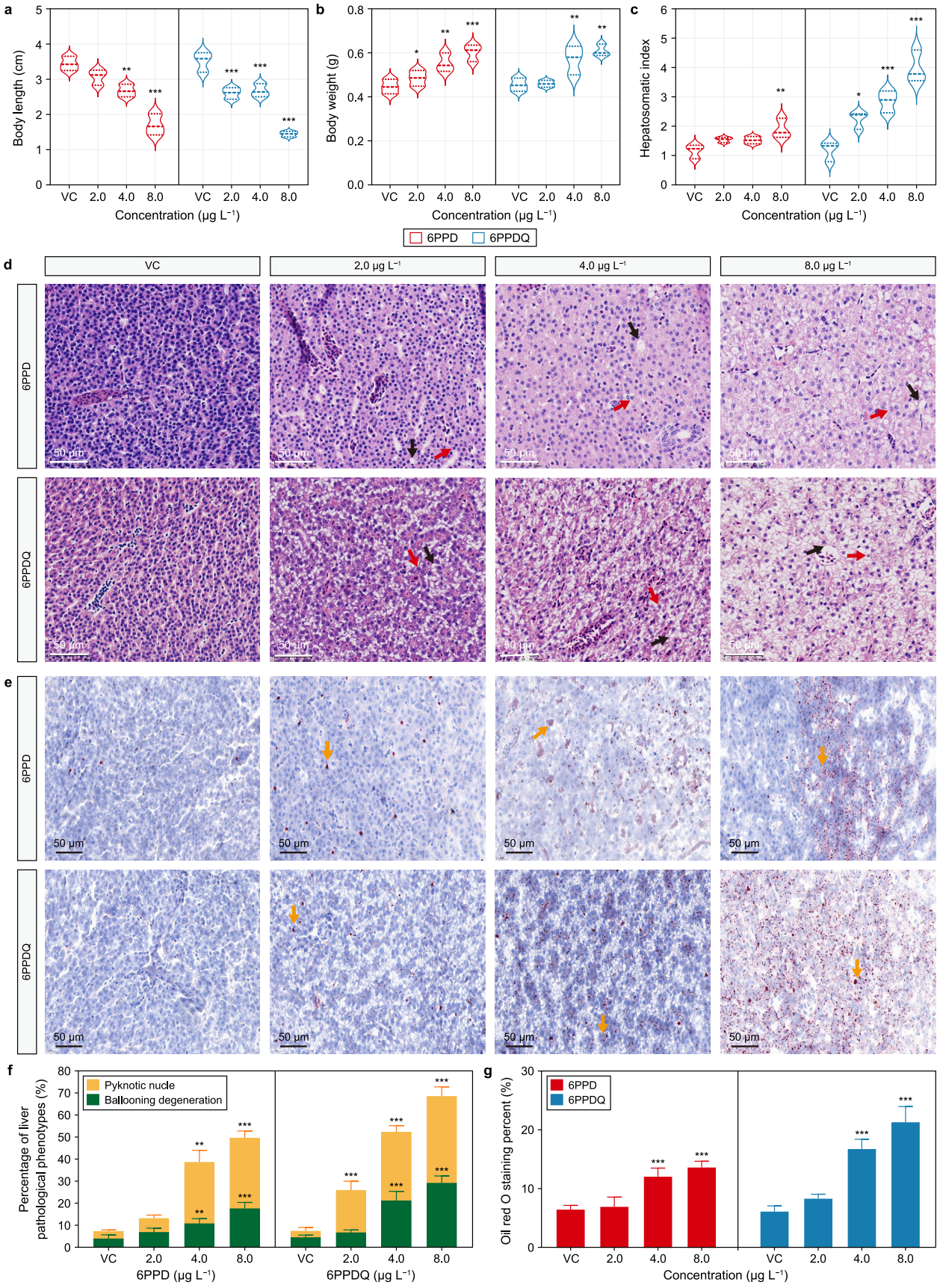

Fig. 2. Growth and hepatic morphological changes in zebrafish after three-month exposure to 6PPD or 6PPDQ. **a**–**c**, Growth parameters following chemical treatments: body length (**a**), body weight (**b**), and hepatosomatic index (**c**). The three dashed lines within each violin plot represent the 25th percentile, median, and 75th percentile, respectively ($n = 3$). **d**, **f**,

fold in the 4 and 8 μg L^{-1} groups, respectively (Fig. 3d–f). In the 6PPDQ exposure groups, both SOD and GSH-Px activities were inhibited at all exposure levels, with 0.80-, 0.58-, and 0.42-fold decreases in SOD; 0.57-, 0.38-, and 0.29-fold decreases in GSH-Px; and 1.28-, 1.81-, and 2.84-fold increases in MDA, which were considered notable (Fig. 3d–f). Moreover, exposure to both 6PPD and 6PPDQ led to significant increases in ROS across all exposure levels, with 6PPD causing increases of 1.32-, 1.47-, and 1.85-fold, and 6PPDQ causing increases of 1.42-, 1.82-, and 2.52-fold compared to those in the VC group (Fig. 3g).

Data for ALT, AST, ALP, SOD, GSH-Px, MDA, and reactive oxygen species (ROS) are presented as star plots (Fig. 3h and i), with zero representing the baseline activity. The plots reveal significant SOD inhibition and ALT activation, along with elevated ROS in both 6PPD- and 6PPDQ-exposure groups. Higher concentrations of 6PPD and 6PPDQ corresponded to increased IBR values (Fig. 3j), thus suggesting greater toxicity in zebrafish, with 6PPDQ having a stronger effect on hepatic toxicity.

3.4. Effects of the exposure of 6PPD and 6PPDQ on the liver transcriptome and metabolism of zebrafish

Transcriptome analysis was conducted to explore the mechanisms of 6PPD- and 6PPDQ-induced hepatic toxicity (Fig. 4). In zebrafish exposed to 6PPD, 1074 differentially expressed genes (DEGs; 531 upregulated, 543 downregulated) were identified; in zebrafish exposed to 6PPDQ, 2780 DEGs (1176 upregulated, 1604 downregulated; Supplementary Material Fig. S2a and b) were identified. Moreover, 356 DEGs were commonly altered between the two groups (Supplementary Material Fig. S3). qRT-PCR validation confirmed a strong correlation ($R^2 > 0.9$) with RNA sequencing results, thus supporting the reliability of the data (Supplementary Material Fig. S4). Gene ontology (GO) analysis revealed significant effects on metabolic processes—including carbohydrate, steroid, and lipid metabolism—in the 6PPD-exposure groups and similar processes—including cholesterol metabolism—in the 6PPDQ-exposure groups (Supplementary Material Fig. S2c and d). The Kyoto Encyclopedia of Gene and Genome (KEGG) pathway analysis (Fig. 4a and b) revealed “Metabolism” as being the most enriched pathway in both groups, including lipid metabolism (steroid biosynthesis, fatty acid biosynthesis, glycerophospholipid, and glycerolipid metabolism) and carbohydrate metabolism (glycolysis/gluconeogenesis, starch, and sucrose metabolism). Additionally, endocrine-related pathways, such as PPAR and insulin (INS) signaling, were enriched in both exposure groups (Fig. 4a and b). Further, key genes from the DEGs related to carbohydrate and lipid metabolism were selected and imported into STRING to construct an interaction network for core protein prediction (Fig. 4c and d). Three topological algorithms—maximal clique centrality (MCC), density of maximum neighborhood component (DMNC), and maximum neighborhood component (MNC)—were employed to identify the top 50 hub genes via the STRING database and CytoHubba plugin in Cytoscape (Supplementary Material Fig. S5). An intersection analysis identified 20 key genes in the 6PPD-exposure group (*fasn*, *pparg*, *pck1*, *g6pca.1*, and *acaca* as the top five core genes) and 37 key genes in the 6PPDQ-exposure group (*fasn*, *pck1*, *acaca*, *pparg*, and *pfklr* as the top five core genes) (Fig. 4c and d). The results revealed distinct response profiles between zebrafish exposed to 6PPD and 6PPDQ.

Based on our transcriptomic results, we investigated the impact of the exposure of 6PPD and 6PPDQ on the metabolic functions of zebrafish. In the 6PPD exposure group, blood INS, adenosine triphosphate (ATP; at 4 and 8 μg L^{-1}), pyruvic acid (PA), and total bile acid (TBA; at 8 μg L^{-1}) levels decreased, while triglycerides (TG), glycogen (at 4 and 8 μg L^{-1}), glucose, total cholesterol (T-CHO), free fatty acid (FFA), and acetyl-CoA levels increased. In the 6PPDQ-exposure group, INS, PA, LA, TBA, and ATP levels were reduced across all exposure groups, whereas glucose, glycogen, TG, FFA, T-CHO, low-density lipoprotein cholesterol (LDL-C), and acetyl-CoA levels increased in all groups, with high-density lipoprotein cholesterol (HDL-C) increasing only at a concentration of 8 μg L^{-1} (Fig. 4e and f).

3.5. Exposure to 6PPD and 6PPDQ altered zebrafish behavior

An open-field test was conducted to evaluate the effects of chemically induced lipid accumulation on zebrafish behavior (Fig. 5). Zebrafish exposed to 6PPD showed a significant, dose-dependent reduction in swimming distance compared to those in the VC group, while the same reduction in zebrafish exposed to 6PPDQ also followed a dose-dependent pattern (Fig. 5a and b). Additionally, exposure to 6PPD significantly increased the time zebrafish spent in darkness, with dwell times at 4 and 8 μg L^{-1} being 1.28 and 1.89 times longer than that of zebrafish in the VC group. In the 6PPDQ-exposure groups, the dwell time in darkness increased by 1.26 times at 2 μg L^{-1}, 1.97 times at 4 μg L^{-1}, and 2.40 times at 8 μg L^{-1} (Fig. 5c). Moreover, the cumulative immobility duration in the light box increased by 1.83 and 2.50 times for zebrafish exposed to 4 and 8 μg L^{-1} of 6PPD, respectively (Fig. 5d). Similarly, in zebrafish exposed to 6PPDQ, the immobility duration increased by 1.73, 2.77, and 3.90 times at 2, 4, and 8 μg L^{-1}, respectively (Fig. 5d).

3.6. Exposure to 6PPD and 6PPDQ disrupted the PPAR signaling pathways of zebrafish

This study employed immunofluorescence localization to investigate the expression of PPARγ, IL-6, and TNF-α in the liver of zebrafish exposed to 6PPD and 6PPDQ. The results revealed a significant dose-dependent decrease in PPARγ expression and a significant increase in the IL-6 and TNF-α levels in the 2, 4, and 8 μg L^{-1} 6PPD-exposure groups (Fig. 6a–c). In the 6PPDQ-exposure groups, there was a dose-dependent increase in PPARγ expression and a significant increase in IL-6 expression across all exposure concentrations. However, TNF-α expression was only elevated in the 4 and 8 μg L^{-1} 6PPDQ groups (Fig. 6b and c).

3.7. Protein-level confirmation of PPAR signaling disruption

Western blot analysis further confirmed the abovementioned findings and revealed significantly lower PPARγ protein levels and significantly higher IL-6 and TNF-α protein levels in the 4 and 8 μg L^{-1} 6PPD-exposure groups (Fig. 7a–c). Similarly, in the 6PPDQ-exposure groups, PPARγ expression was significantly reduced at all concentrations, with IL-6 and TNF-α levels significantly increased in the 4 and 8 μg L^{-1} groups (Fig. 7b and c).

Liver sections stained with hematoxylin-eosin (**d**) and oil red O (**f**). **e**, **g**, Quantification of hematoxylin-eosin-positive areas (**e**) and oil red O-stained areas (**g**). Black arrows indicate lipid vacuoles, red arrows indicate pyknotic nuclei, and yellow arrows indicate lipid droplets. Values are presented as mean ± standard deviation ($n = 3$). *$P < 0.05$, **$P < 0.01$, ***$P < 0.001$ indicate statistically significant differences compared to vehicle control (VC).

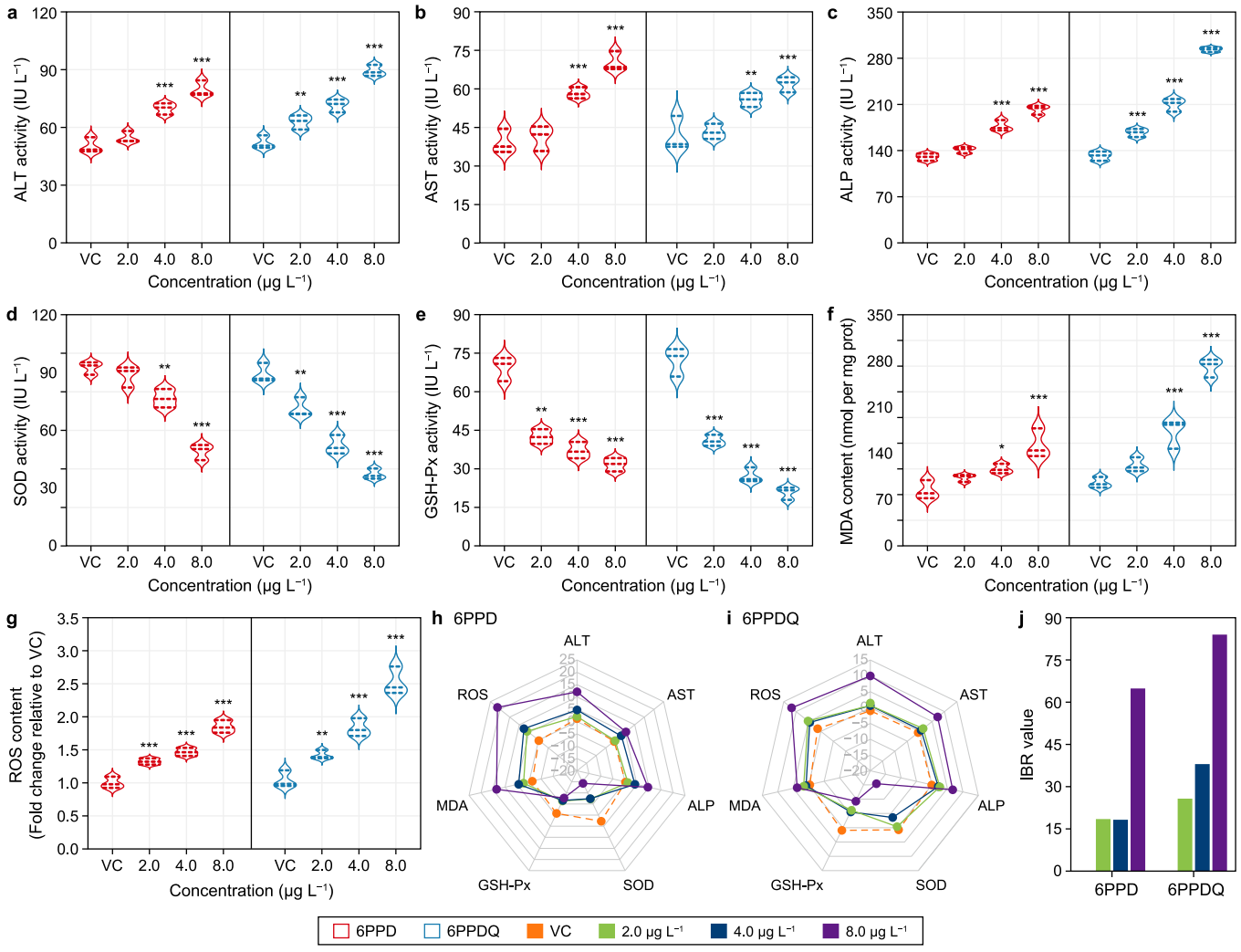

Fig. 3. Hepatic toxicity biomarker responses in zebrafish after three-month exposure to 6PPD or 6PPDQ. **a**–**c**, Liver function indices: alanine aminotransferase (ALT, **a**), aspartate aminotransferase (AST, **b**), and alkaline phosphatase (ALP, **c**) activities. **d**–**g**, Antioxidant indicators in the liver: superoxide dismutase (SOD, **d**), glutathione peroxidase (GSH-Px, **e**) activity, malondialdehyde (MDA, **f**) content, and reactive oxygen species (ROS, **g**) content. The three dashed lines within each violin plot represent the 25th percentile, median, and 75th percentile, respectively ($n = 3$). **h**–**i**, Radar plots of liver indicators following exposure to 6PPD (**h**) and 6PPDQ (**i**). **j**, Integrated biomarker response analysis (IBR) values. $^{*}P < 0.05$, $^{**}P < 0.01$, $^{***}P < 0.001$ indicate statistically significant differences compared to vehicle control (VC).

3.8. Binding modes and kinetics of 6PPD and 6PPDQ to PPARγ

3.8.1. Homology modeling and molecular docking

The homology modeling results for zebrafish PPARγ (zfPPARγ) are depicted in Fig. S6a (Supplementary Material). The Ramachandran plot revealed that only two residues are located in disallowed regions; this suggests a reasonable protein structure of zfPPARγ (Supplementary Material Fig. S6b). The sequence identity between zfPPARγ and the homology template is 73%, which indicates a high degree of similarity and that the constructed protein structure closely matches the secondary structure tendencies of the template (Supplementary Material Fig. S6c and d). In addition, the QMEANDisCo Global score of 0.70 ± 0.05 (on a scale from 0 to 1) further supports the model quality.

To evaluate the overall structural alterations in the chemical–protein complexes, the conformations at 0 and 200 ns were analyzed (Supplementary Material Fig. S7a; Fig. 8a). After 200 ns, both 6PPD and 6PPDQ were found to shift closer to the β-sheet junction of the zfPPARγ subunit, suggesting a relocation of their interaction sites. The interaction between 6PPD and PPARγ primarily involved hydrophobic interactions and van der Waals forces, with the benzene rings and alkyl groups of 6PPD interacting with residues Pro271, Leu272, Leu383, Arg338, Ala342, Ile380, Met414, and Ile391. 6PPDQ also formed hydrophobic interactions; specifically, a nitrogen atom of 6PPDQ formed a conventional hydrogen bond with Arg338. The benzoquinone ring, benzene ring, and alkyl group of 6PPDQ interacted with the residues Met379, Pro271, Ala342, Ile380, Leu299, Ile391, and Met398. The analysis indicated that both 6PPD and 6PPDQ induced significant conformational changes in the three-dimensional structure of zfPPARγ.

3.8.2. Binding-free energy

The binding-free energies of 6PPD and 6PPDQ with zfPPARγ were calculated using the molecular mechanics Poisson–Boltzmann surface area (MM-PBSA) method to assess binding strength and affinity (Supplementary Material Fig. S7b). The binding-free energy ($\Delta G_{binding}$) comprises van der Waals energy (ΔE_{vdw}), electrostatic energy (ΔE_{ele}), polar solvation energy (ΔG_{polar}), and nonpolar solvation energy ($\Delta G_{nonpolar}$). The results indicated that van der Waals energy (ΔE_{vdw}) is the largest

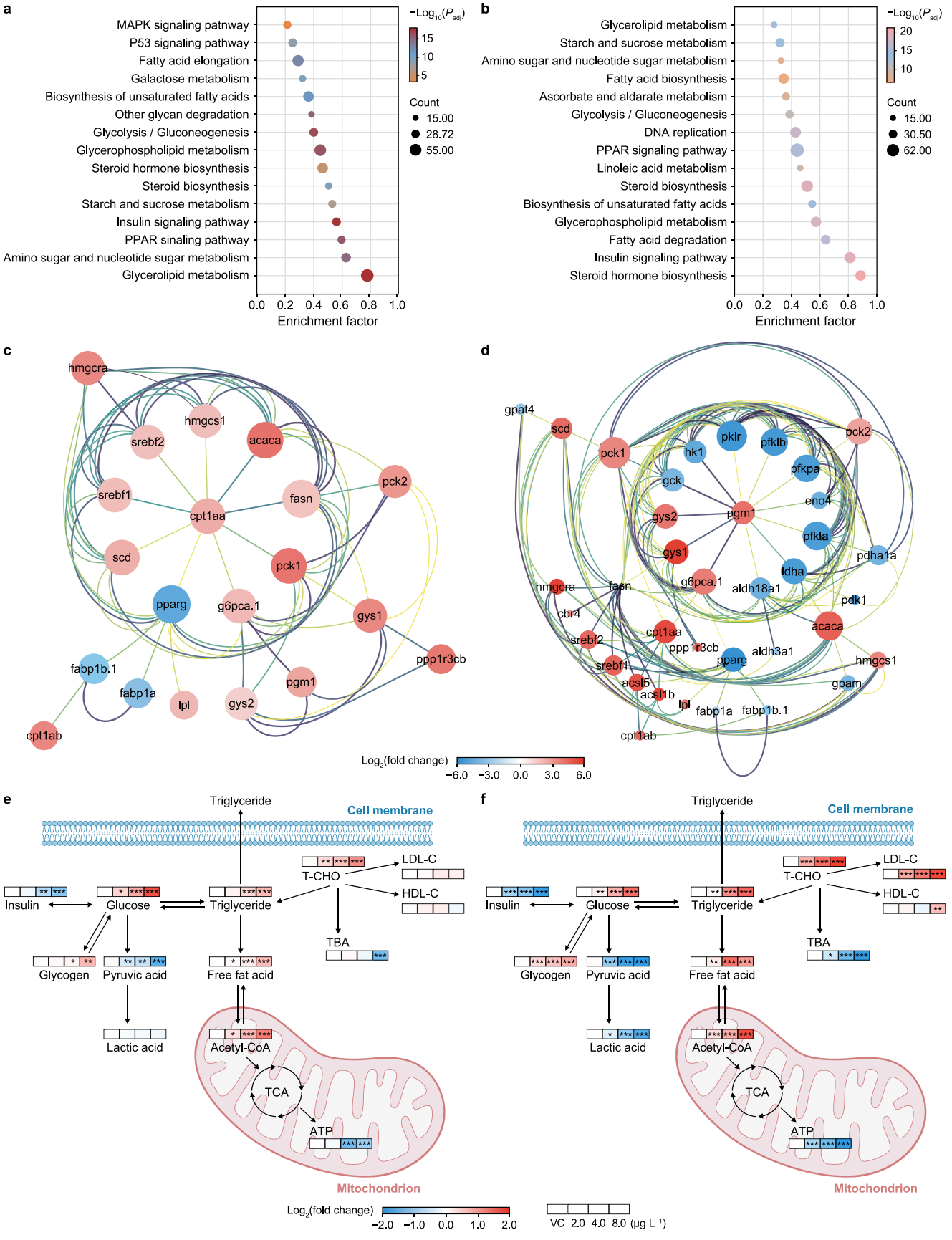

Fig. 4. Transcriptome analysis. **a**–**b**, Top 15 enriched KEGG pathway analysis of DEGs in the 6PPD (**a**) and 6PPDQ (**b**) groups. P_{adj}: adjusted *P*-value. **c**–**d**, Protein interaction networks for 6PPD (**c**) and 6PPDQ (**d**). The node's size represents the protein's importance or the degree of connectivity with other proteins. **e**–**f**, Coregulatory networks of liver glucose and

contributor in both 6PPD-zfPPARγ and 6PPDQ-zfPPARγ complexes, with values of −40.79 and −44.49 kcal mol^{-1}, respectively. Additionally, electrostatic energy, polar solvation energy, and nonpolar solvation energy contributed to binding affinity. The absolute binding-free energies ($\Delta G_{binding}$) for 6PPD and 6PPDQ were −24.65 and −22.88 kcal mol^{-1}, respectively, thereby indicating that 6PPD exhibited slightly stronger binding affinity to zfPPARγ compared to that of 6PPDQ. Further, energy decomposition analysis identified Leu383 as the key residue that contributed to the binding of 6PPD, with an energy value of −1.33 kcal mol^{-1} (Supplementary Material Fig. S7c), while Ile391 was the predominant residue that contributed to the binding of 6PPDQ, with a binding energy of −1.56 kcal mol^{-1} (Supplementary Material Fig. S7d).

3.8.3. Simulation of molecular dynamics

Complex models of zfPPARγ with 6PPD and 6PPDQ were subjected to 200 ns of MD simulation. The root mean square deviation (*RMSD*) values of the protein-ligand complexes (Fig. 8b and c), indicate that both systems reached equilibrium after approximately 25 ns. During the remaining 175 ns, minimal fluctuations were observed, which suggested stability throughout the simulation period. The root mean square fluctuation (*RMSF*) values of zfPPARγ residues after binding with 6PPD or 6PPDQ are illustrated in Fig. 8d, thus reflecting residue flexibility. The results indicate greater residue fluctuation in zfPPARγ bound to 6PPDQ compared to zfPPARγ bound to 6PPD.

3.8.4. Binding kinetics

The binding kinetics and affinity of 6PPD and 6PPDQ to hPPARγ were confirmed using the SPR technique. GW9662 was employed as a positive control, thereby demonstrating dose-dependent binding to hPPARγ (Fig. 8e). Both 6PPD and 6PPDQ also exhibited dose-dependent binding to hPPARγ. 6PPD showed a slow association rate, but dissociated quickly from hPPARγ (Fig. 8f); in contrast, 6PPDQ displayed fast association and dissociation rates from the hPPARγ surface (Fig. 8g). Further, the equilibrium dissociation constants (KD) for GW9662, 6PPD, and 6PPDQ were 8.76×10^{-7}, 6.83×10^{-6}, and 4.47×10^{-7} M, respectively.

4. Discussion

In this study, zebrafish were used as a model to assess the chronic toxicity of 6PPD and its oxidation product—6PPDQ. The underlying molecular mechanisms were comprehensively investigated using various analytical and molecular techniques. Our results demonstrated that the liver is the primary site of 6PPD bioaccumulation, while the brain is the main site of 6PPDQ bioaccumulation. Exposure to environmentally relevant concentrations of 6PPD and 6PPDQ led to significant disruptions in lipid and carbohydrate metabolism, downregulation of PPARγ, and increased levels of pro-inflammatory cytokines, such as TNF-α and IL-6. Overall, these findings indicate that 6PPD and 6PPDQ pose a significant risk of chronic hepatotoxicity to aquatic organisms, with 6PPDQ demonstrating greater toxicity.

4.1. Bioaccumulation patterns

Our results revealed that 6PPD primarily accumulates in the liver and gonads of zebrafish, whereas 6PPDQ preferentially accumulates in the brain at levels that are 5.14 times higher than those of 6PPD. This aligns with recent findings that 6PPDQ tends to accumulate in the brain [21], possibly due to their differing physicochemical properties [33,34]. The lipophilic nature of 6PPD leads to its accumulation in fatty tissues [35,36], while the polarity of 6PPDQ enables it to cross the blood–brain barrier [37], thereby raising concerns regarding its neurotoxic potential [21,38]. These observations highlight the importance of assessing both parent compounds and their transformation products, as they can significantly alter the target organ accumulation and toxicity profiles.

4.2. Hepatotoxic effects

The liver plays a critical role in the bioaccumulation, metabolism, and detoxification of xenobiotics, thereby making it particularly vulnerable to environmental pollutants [39]. In our study, exposure to 6PPDQ was found to lead to more severe hepatic damage than exposure to 6PPD—as evidenced by increased HSI, ballooning degeneration, and nuclear pyknosis—despite lower accumulation levels of 6PPDQ in the liver [40]. These findings are consistent with previous studies that indicate that 6PPDQ can cause significant liver damage, including reduced hepatocyte space and nuclear abnormalities [19,37,41]. Furthermore, Oil Red O staining demonstrated that exposure to both 6PPD and 6PPDQ resulted in increased lipid droplet accumulation in zebrafish hepatocytes, indicative of non-alcoholic fatty liver disease (NAFLD) [42,43]. Although 6PPD exhibited approximately 1.64 times higher liver bioaccumulation than 6PPDQ, the greater severity of toxic effects observed with 6PPDQ suggests that it may possess stronger hepatotoxic potential, possibly due to differences in the molecular mechanisms of action between 6PPD and 6PPDQ.

Given the liver's central role in fat and carbohydrate metabolism, we measured several liver function parameters, including enzyme levels of ALT, AST, and ALP [44]. ALT and AST are essential biochemical markers of liver injury because they are released into the bloodstream when liver damage occurs [45–47]. Additionally, ALT levels are linked to fat accumulation in the liver. Moreover, ALP can be used as a biochemical marker of liver diseases, particularly cholestatic conditions. In our study, significant increases in ALT, AST, and ALP levels were observed in both the 6PPD and 6PPDQ exposure groups, thereby indicating significant hepatic damage in zebrafish. This damage was further associated with oxidative stress, as evidenced by the overproduction of ROS in the present study, which is a critical factor in hepatic damage and directly reflects the extent of oxidative stress [48,49]. Typically, endogenous antioxidant enzymes—such as SOD and GSH-Px—mitigate oxidative stress, with the SOD system providing the first line of defense against ROS [50,51]. However, the observed reduction in SOD and GSH-Px activities suggests that the antioxidant defenses in zebrafish were overwhelmed, thereby leading to excessive ROS production and resulting in oxidative damage. Further, elevated levels of MDA, a product of lipid peroxidation, confirmed the occurrence of oxidative damage and, thus, indicated significant lipid peroxidation [52–54]. These observations align with oxidative stress and lipid perturbations reported in other organisms—including *Pimephales promelas*, *C.elegans*, *O. mykiss*, and *Chlorella vulgaris*—and emphasize the broad impacts of 6PPD and 6PPDQ exposure on aquatic organisms [37,55–58]. Furthermore, IBR analysis revealed that the toxic effects of 6PPDQ on the liver were significantly greater than those of 6PPD.

lipid metabolism in 6PPD (**e**) and 6PPDQ (**f**). T-CHO: total cholesterol. LDL-C: low-density lipoprotein cholesterol. HDL-C: high-density lipoprotein cholesterol. TBA: total bile acid. TCA: Tricarboxylic acid cycle. ATP: adenosine triphosphate. Red indicates upregulation and blue indicates downregulation, with intensity reflecting $\log_2$(fold change). $^{*}P < 0.05$, $^{**}P < 0.01$, $^{***}P < 0.001$ indicate statistically significant differences compared to vehicle control (VC).

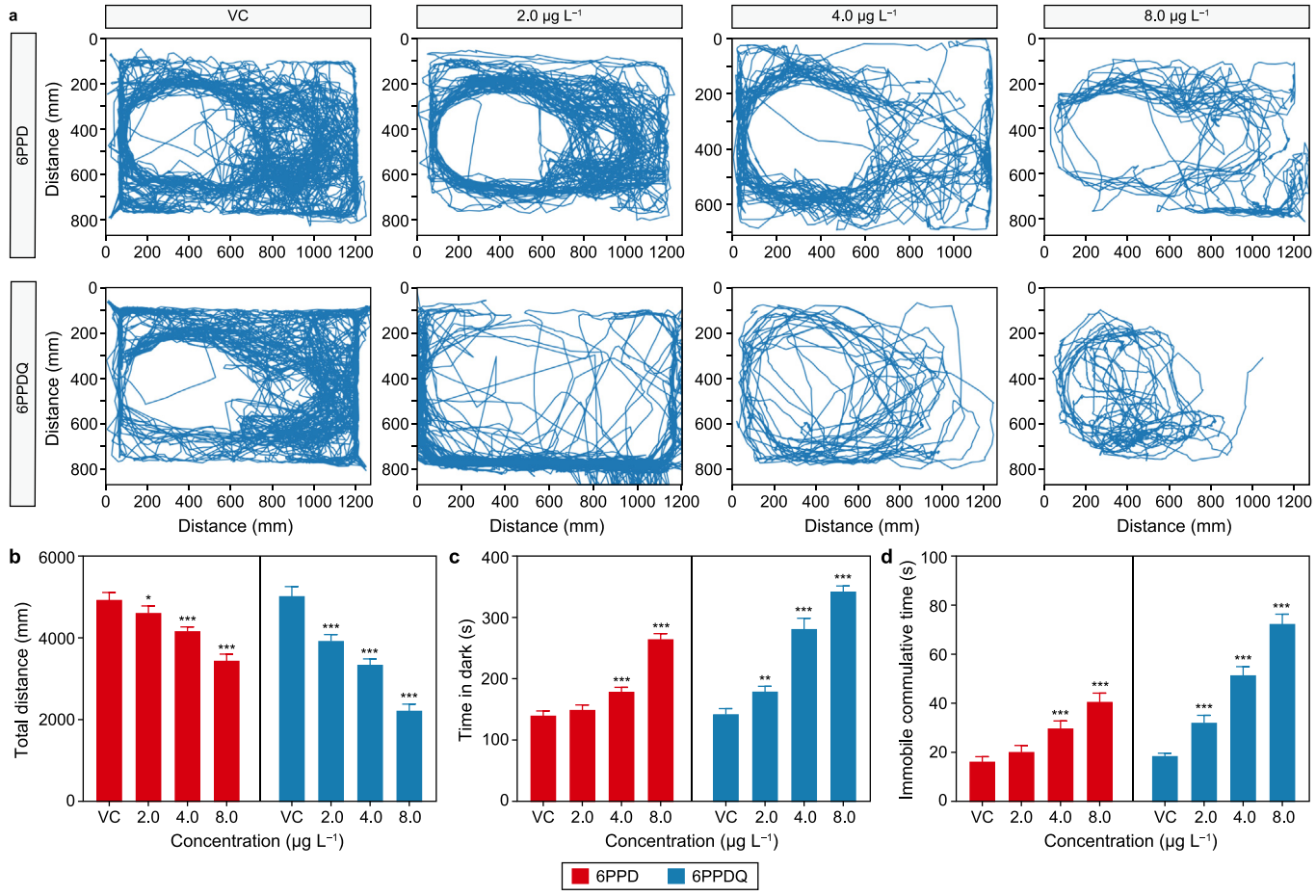

Fig. 5. Behavioral responses of zebrafish following three-month exposure to 6PPD or 6PPDQ. **a**, Representative movement trajectory in the open field test. **b**, Swimming distance. **c**, Dwell time in the dark zone. **d**, Cumulative immobile duration in the light. Values are presented as mean ± standard deviation. *$P < 0.05$, **$P < 0.01$, ***$P < 0.001$ indicate statistically significant differences compared to vehicle control (VC).

4.3. Molecular mechanisms

RNA sequencing analysis indicated that exposure to 6PPD and 6PPDQ disrupts lipid and carbohydrate metabolism pathways, ultimately leading to hepatocyte injury. The distinct molecular responses between the 6PPD and 6PPDQ exposure groups highlighted the potential for differential toxicity mechanisms, with 6PPDQ exhibiting a greater impact on lipid biosynthesis and glycolytic inhibition. In lipid metabolism, genes involved in de novo fatty acid biosynthesis—such as *acaca*, *scd*, and *fasn*—were found to be upregulated, thus reflecting increased lipogenesis [59]. Similarly, the upregulation of *lpl*—an encoding lipoprotein lipase, a key enzyme in lipid metabolism—suggests elevated hydrolysis of triglycerides [60]. In parallel, *cpt1a*—the gene encoding the rate-limiting enzyme of mitochondrial β-oxidation—was also upregulated, with both isoforms *cpt1aa* and *cpt1ab* showing increased expression [61]. This suggests that zebrafish responded to lipid accumulation by accelerating fatty acid β-oxidation as a compensatory mechanism to maintain lipid homeostasis. Additionally, the upregulation of fatty acid biosynthesis genes *acsl1b*, *acsl5*, and *cbr4* was specifically observed in the 6PPDQ group, thereby indicating a more pronounced activation of fatty acid synthesis compared to that caused by 6PPD exposure [62]. Further, cholesterol metabolism was also affected, as evidenced by the upregulation of cholesterol biosynthesis genes—including *hmgcra*, *hmgcs1*, *srebf1*, and *srebf2*—thereby suggesting increased cholesterol production [63,64]. Meanwhile, the concurrent downregulation of *pparγ* (*pparg*) and its downstream target *fabp1* (including isoforms *fabp1a* and *fabp1b.1*)—in addition to the presence of hepatic steatosis—suggested that a negative feedback mechanism was triggered in response to excessive lipid accumulation [65,66]. Notably, the exclusive downregulation of *gpat4* and *gpam* in the 6PPDQ group implies that 6PPDQ may specifically inhibit glycerolipid metabolism [67,68]. Significant disruptions were observed in carbohydrate metabolism, particularly in glycolysis and glycogenesis. In the 6PPDQ group, glycolysis-related genes—including *pdk1*, *pklr*, *gck*, *pfkla*, *pfklb*, *hk1*, *eno4*, *pfkpa*, *aldh3a1*, *aldh18a1*, *ldha*, and *pdha1a*—were downregulated. Since *hk1* and *gck* play essential roles in glucose metabolism and INS secretion, their suppression suggests that 6PPDQ-induced metabolic disturbances may impair the INS signaling pathway and, thus, lead to imbalances in glucose-lipid homeostasis [69,70]. In contrast, genes involved in glycogenesis—such as *g6pca.1*, *ppp1r3cb*, *gys1*, *gys2*, *pgm1*, and *pck1*—were upregulated in both the 6PPD- and 6PPDQ-exposure groups, thereby indicating that these chemicals may promote glycogen synthesis by activating key enzymes [71]. These findings suggest that prolonged exposure to 6PPDQ disrupts hepatic glucose metabolism by inhibiting glycolysis, while inducing lipid accumulation and alterations in cholesterol homeostasis.

Biochemical indicators further confirmed these metabolic disruptions. Specifically, decreased INS, ATP, PA, and TBA levels indicated impaired energy metabolism and hepatic function [72,73]. In

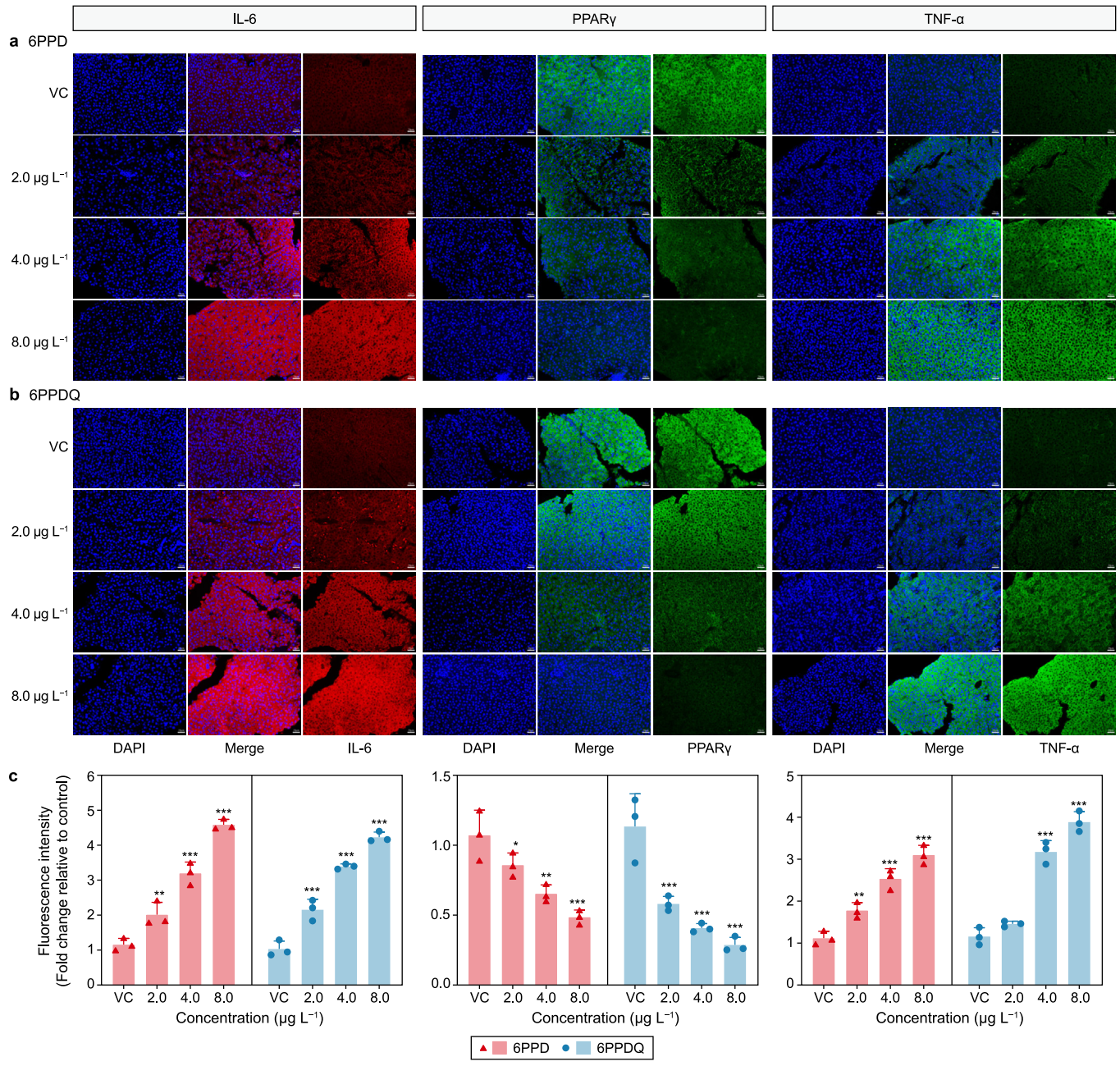

Fig. 6. Effects of 6PPD or 6PPDQ on liver inflammation indicators after three-month exposure in zebrafish. **a**–**b**, Immunofluorescence staining for interleukin-6 (IL-6), peroxisome proliferator-activated receptor gamma (PPARγ), and tumor necrosis factor-alpha (TNF-α) in the 6PPD (**a**) and 6PPDQ (**b**) groups. **c**, Fluorescence intensity of IL-6, PPARγ, and TNF-α. Values are presented as mean ± standard deviation. *$P < 0.05$, **$P < 0.01$, ***$P < 0.001$ indicate statistically significant differences compared to vehicle control (VC).

contrast, increased TG, glycogen, glucose, and FFA levels suggested lipid accumulation and glucose dysregulation conditions linked to NAFLD [74,75]. The reduction in ATP levels also indicated mitochondrial dysfunction, which may exacerbate oxidative stress and contribute to liver damage [76,77]. Moreover, elevated LDL-C levels in the 6PPDQ-exposure group suggest more severe hepatic damage, whereas increased HDL-C at higher exposure levels may represent a compensatory mechanism for lipid transport [78,79]. These disruptions in lipid and carbohydrate metabolism due to 6PPD and 6PPDQ exposure suggest potential liver disease in zebrafish.

Locomotor activity is generally considered a sensitive indicator of neurobehavior, but it also requires sufficient ATP availability; thus, it is regarded as an important marker of energy metabolism [80,81]. In fish, lipids provide nutrients, serve as an energy source, and contribute to cellular structures [82]. Logically, lipid accumulation would contribute to an increase in ATP production and swimming activity. However, this study observed reduced locomotor performance and decreased ATP levels, suggesting that lipid accumulation did not enhance ATP production as anticipated. ATP production is an important endpoint of mitochondrial energy metabolism [81]. Therefore, the observed changes in ATP content and locomotor performance suggest that 6PPD and 6PPDQ might induce mitochondrial dysfunction, thereby impairing the energy supply necessary for normal motor activity. Furthermore, the increased dwell time in darkness and prolonged immobility observed in zebrafish exposed to both 6PPD and 6PPDQ indicate an

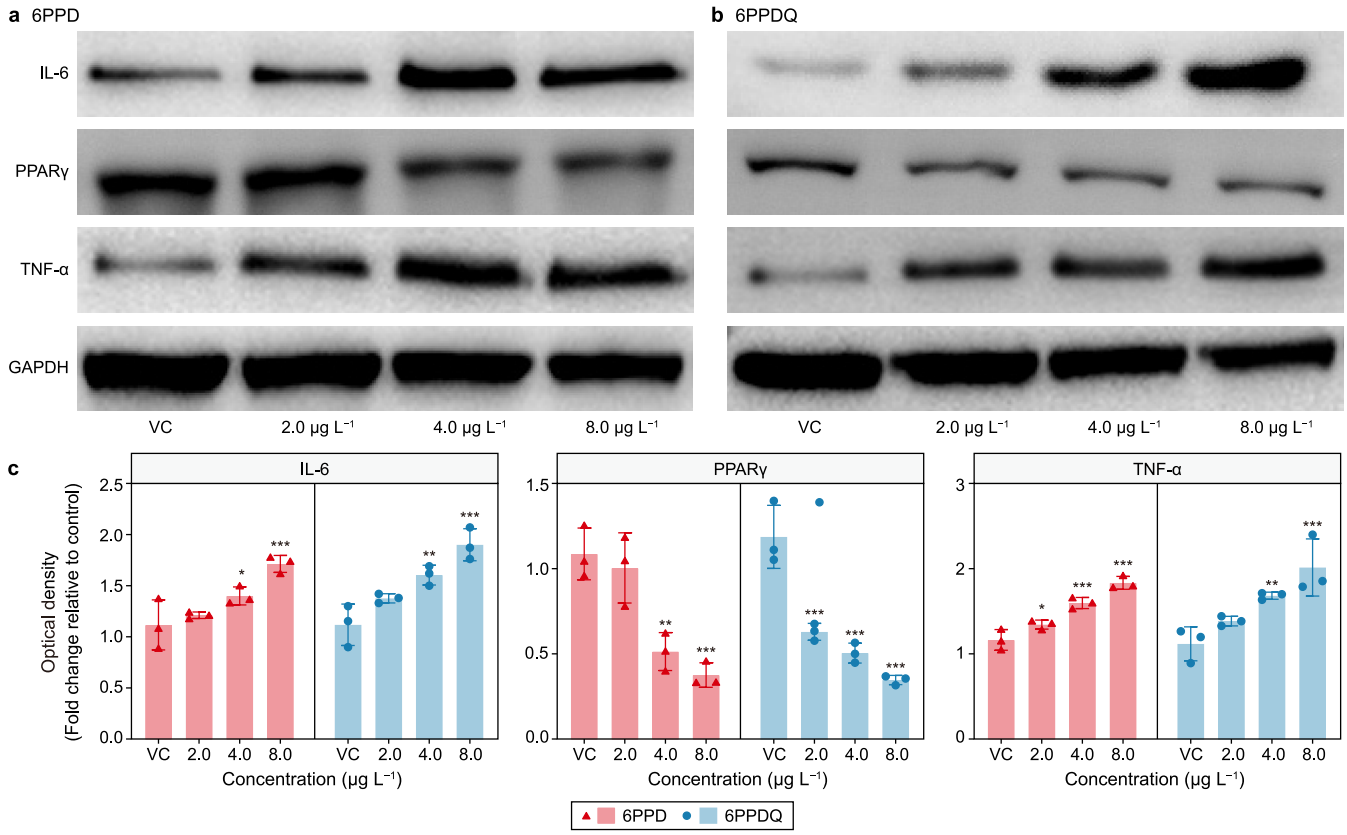

Fig. 7. **a**–**b**, Western blot analysis of interleukin-6 (IL-6), peroxisome proliferator-activated receptor gamma (PPARγ), and tumor necrosis factor-alpha (TNF-α) in the 6PPD (**a**) and 6PPDQ (**b**) groups. **c**, Relative protein expression levels of IL-6, PPARγ, and TNF-α. Values are presented as mean ± standard deviation. *$P < 0.05$, **$P < 0.01$, ***$P < 0.001$ indicate statistically significant differences compared to vehicle control (VC).

anxiety-like phenotype [83], which is potentially linked to elevated oxidative stress and disruptions in the PPARγ signaling pathway [84–86]. These findings highlight the complex interplay among energy homeostasis, oxidative stress, and signaling pathway disturbances in mediating the behavioral toxicity of both 6PPD and 6PPDQ.

4.4. PPARγ and inflammatory signaling

These metabolic perturbations establish a mechanistic link to inflammation. Excessive lipid accumulation and disruptions in glucose metabolism are well-documented triggers of inflammatory responses [87–89]. PPARγ—a key nuclear receptor and transcription factor involved in lipid metabolism—regulates genes associated with lipid transport, synthesis, lipolysis, and storage [66,90]. PPARγ also plays an essential anti-inflammatory role by promoting macrophage polarization toward the M2 phenotype, suppressing pro-inflammatory cytokine production [91]. In our study, exposure of zebrafish to 6PPD and 6PPDQ led to a marked downregulation of PPARγ at both the protein and transcriptional levels, thereby suggesting that these chemicals directly target the PPAR signaling pathway and, thus, disrupt lipid metabolism and inflammatory regulation. As expected, both 6PPD and 6PPDQ exposure significantly increased TNF-α and IL-6 expression, indicating enhanced hepatic inflammation due to reduced PPARγ levels. IL-6 and TNF-α are key pro-inflammatory cytokines that regulate immune responses, promote inflammatory processes, contribute to metabolic dysfunction, and drive the progression of nonalcoholic steatohepatitis [92]. Given that inflammation and hepatocyte injury are hallmarks of steatohepatitis, our results suggest that 6PPD and 6PPDQ exposure may contribute to this pathology. Similarly, a previous study reported that 6PPDQ induces immune responses and macrophage infiltration in mouse livers [19], further supporting our findings in zebrafish. These results also align with our histological observations, which revealed inflammatory cell infiltration in the liver.

To further investigate the underlying mechanisms, we employed MD simulations and SPR to examine the binding affinity of 6PPD and 6PPDQ to PPARγ, as these are reliable tools for studying the interactions between chemicals and proteins [93,94]. The MD simulations revealed greater residue fluctuations in PPARγ when bound to 6PPDQ compared to when bound to 6PPD, thus suggesting that 6PPDQ induces more significant conformational changes that may impair protein function [95]. Correspondingly, SPR results confirmed that 6PPDQ has a stronger binding affinity to PPARγ than 6PPD, as evidenced by a lower KD value [96]. This difference in binding affinity may explain the greater hepatotoxicity of 6PPDQ, although 6PPD exhibits higher liver accumulation.

5. Conclusion

Our study demonstrated that exposure to 6PPD and 6PPDQ at environmentally relevant concentrations poses a significant risk of internal accumulation and results in chronic toxic effects in the liver of zebrafish. Toxicokinetics revealed preferential accumulation of 6PPD in the liver and preferential accumulation of 6PPDQ in the brain of zebrafish. Both compounds were shown to induce hepatic injury, with 6PPDQ causing more pronounced damage, as

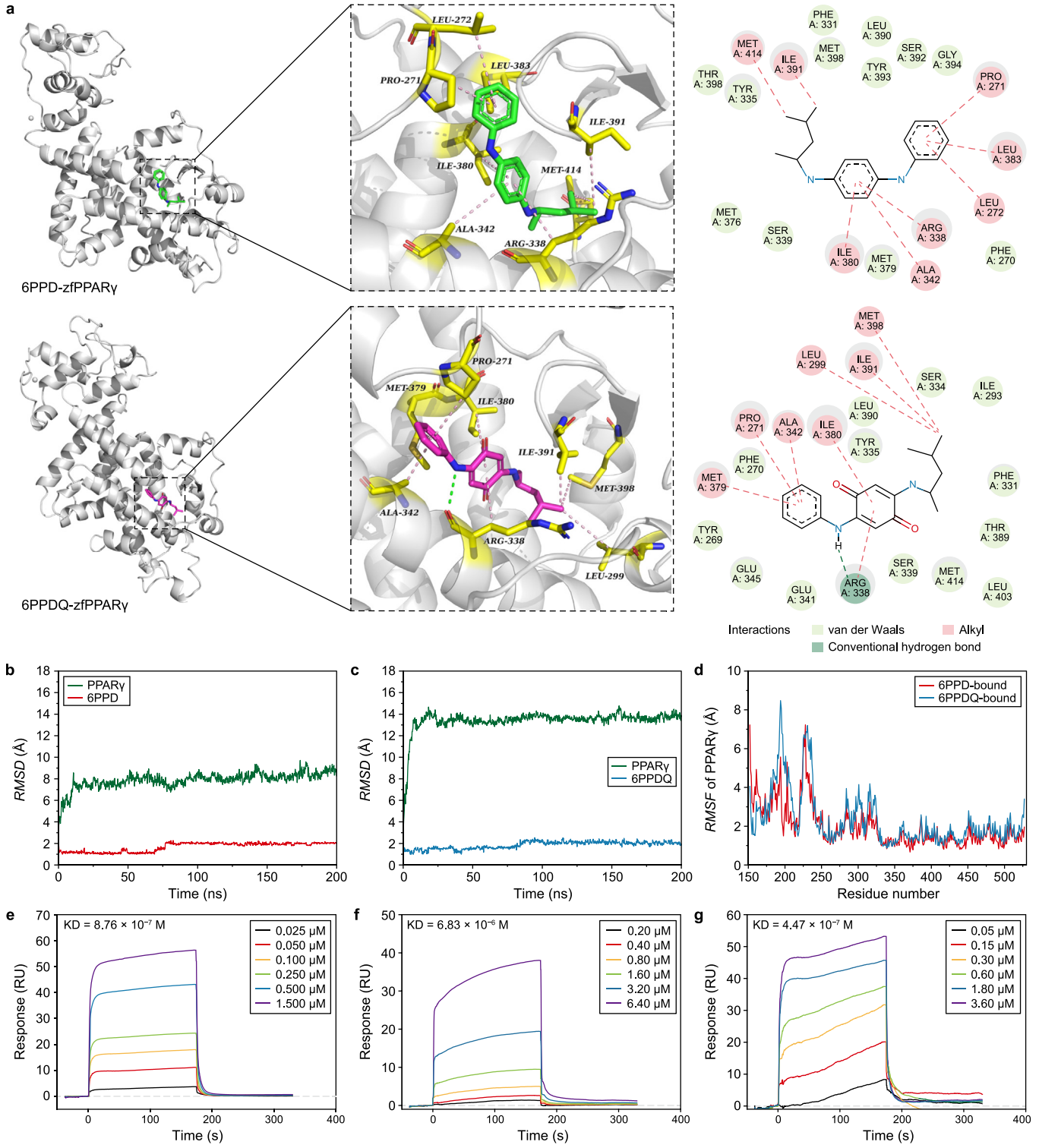

Fig. 8. Molecular interactions between 6PPD or 6PPDQ and peroxisome proliferator-activated receptor gamma (PPARγ). **a**, Conformations of 6PPD-zfPPARγ and 6PPDQ-zfPPARγ at 200 ns. Residues highlighted in dark gray circles represent amino acids involved in hydrophobic interactions with the ligand, without forming explicit hydrogen bonds or other specific interactions. **b**–**c**, Root mean square deviation (*RMSD*) changes over time in 6PPD-zfPPARγ (**b**) and 6PPDQ-zfPPARγ (**c**). **d**, Root mean square fluctuation (*RMSF*) curves. **e**–**g**, Surface plasmon resonance sensorgrams for GW9662 (a PPARγ antagonist, **e**), 6PPD (**f**), and 6PPDQ (**g**) binding to hPPARγ. KD: the equilibrium dissociation constant. zfPPARγ: zebrafish PPARγ. hPPARγ: human PPARγ.

evidenced by morphological changes in the liver and altered biochemical markers. Additionally, both chemicals were found to disrupt lipid and carbohydrate metabolism and upregulate pro-inflammatory cytokines, such as TNF-α and IL-6, thus potentially leading to hepatic inflammation and an increased risk of liver disease. These toxic effects may be related to the differential binding interactions of 6PPD and 6PPDQ with PPARγ. This study underscores the significance of evaluating both parent compounds and their metabolites in environmental toxicity assessments, given the potential of transformation products to significantly alter toxicity profiles. Future studies should focus on the effects of chronic exposure to 6PPD and 6PPDQ, particularly concerning organ-specific toxicities and other adverse outcomes in zebrafish. Due to the conservation of metabolic processes across vertebrates, these findings raise concerns regarding potential health risks for humans, particularly from chronic exposure to rubber-derived contaminants, thereby highlighting the need for regulatory scrutiny and improved water treatment solutions.

CRediT authorship contribution statement

Fang Jiao: Writing - Original Draft, Visualization, Validation, Software, Methodology, Investigation, Funding Acquisition, Data Curation, Conceptualization. **Yang Zhao:** Software, Methodology, Investigation. **Qiang Yue:** Writing - Review & Editing. **Qi Wang:** Validation, Investigation. **Zhongzhi Li:** Methodology, Investigation. **Wanjing Lin:** Software, Methodology. **Lingxi Han:** Writing - Review & Editing, Supervision. **Liangfu Wei:** Writing - Review & Editing, Resources, Project Administration, Methodology.

Declaration of competing interest

The authors declare that they have no known competing financial interests or personal relationships that could have appeared to influence the work reported in this paper.

Acknowledgements

This work was financially supported by the China Postdoctoral Science Foundation (No. 2023M741216), Guangdong Basic and Applied Basic Research Foundation (No. 2023A1515110978; 2024A1515012900), the National Natural Science Foundation of China (No. 32401410), Research Fund Program of Guangdong-Hong Kong Joint Laboratory for Water Security (No. GHJLWS-07), and Xiamen Key Laboratory of Intelligent Fishery (No. XMKLIF-OP-202304). We are grateful to Mr. Jianfeng Yan for his assistance and valuable suggestions during data analysis. We also extend our heartfelt thanks to all laboratory members for their technical support and contributions during sample collection and data analysis. Special thanks go to Dr. Frederik Zietzschmann (Technische Universität Berlin, Germany) for his thorough review and constructive feedback on the manuscript, significantly enhancing its clarity and overall quality.

Appendix A. Supplementary data

Supplementary data to this article can be found online at https://doi.org/10.1016/j.ese.2025.100567.

References

[1] B. Seiwert, M. Nihemaiti, M. Troussier, et al., Abiotic oxidative transformation of 6-PPD and 6-PPD quinone from tires and occurrence of their products in snow from urban roads and in municipal wastewater, Water Res. 212 (2022) 118122.
[2] C. Johannessen, P. Helm, C.D. Metcalfe, Detection of selected tire wear compounds in urban receiving waters, Environ. Pollut. 287 (2021) 117659.
[3] G. Cao, W. Wang, J. Zhang, et al., New evidence of rubber-derived quinones in water, air, and soil, Environ. Sci. Technol. 56 (7) (2022) 4142–4150.
[4] W. Huang, Y. Shi, J. Huang, et al., Occurrence of substituted p-phenylenediamine antioxidants in dusts, Environ. Sci. Technol. Lett. 8 (5) (2021) 381–385.
[5] H.N. Zhao, X. Hu, Z. Tian, et al., Transformation products of tire rubber antioxidant 6PPD in heterogeneous gas-phase ozonation: identification and environmental occurrence, Environ. Sci. Technol. 57 (14) (2023) 5621–5632.
[6] B. Seiwert, P. Klöckner, S. Wagner, et al., Source-related smart suspect screening in the aqueous environment: search for tire-derived persistent and mobile trace organic contaminants in surface waters, Anal. Bioanal. Chem. 412 (2020) 4909–4919.
[7] Z. Tian, H. Zhao, K.T. Peter, et al., A ubiquitous tire rubber-derived chemical induces acute mortality in coho salmon, Science 371 (6525) (2021) 185–189.
[8] X. Chen, T. He, X. Yang, et al., Analysis, environmental occurrence, fate and potential toxicity of tire wear compounds 6PPD and 6PPD-quinone, J. Hazard. Mater. 452 (2023) 131245.
[9] H.Y. Zhang, Z. Huang, Y.H. Liu, et al., Occurrence and risks of 23 tire additives and their transformation products in an urban water system, Environ. Int. 171 (2023) 107715.
[10] H. Chen, M. Xie, W. Li, et al., Detection of 6-PPD and 6-PPDQ in airborne particulates and assessment of their toxicity in lung cells, Chemosphere 364 (2024) 143205.
[11] J. Ji, C. Li, B. Zhang, et al., Exploration of emerging environmental pollutants 6PPD and 6PPDQ in honey and fish samples, Food Chem. 396 (2022) 133640.
[12] Y. Wang, R. Fu, X. Li, et al., Potential thyroid hormone disorder risks of tire antioxidants to aquatic food chain organisms after absorbing free radicals in marine and freshwater environments, Aquat. Toxicol. 260 (2023) 106587.
[13] X. Hua, X. Feng, G. Liang, et al., Exposure to 6-PPD quinone at environmentally relevant concentrations causes abnormal locomotion behaviors and neurodegeneration in *Caenorhabditis elegans*, Environ. Sci. Technol. 57 (12) (2023) 4940–4950.
[14] X. Hua, D. Wang, Exposure to 6-PPD quinone at environmentally relevant concentrations inhibits both lifespan and healthspan in *Caenorhabditis elegans*, Environ. Sci. Technol. 57 (48) (2023) 19295–19303.
[15] S.Y. Zhang, X. Gan, B. Shen, et al., 6PPD and its metabolite 6PPDQ induce different developmental toxicities and phenotypes in embryonic zebrafish, J. Hazard. Mater. 455 (2023) 131601.
[16] C. Fang, L. Fang, S. Di, et al., Characterization of N-(1,3-dimethylbutyl)-N′-phenyl-p-phenylenediamine (6PPD)-induced cardiotoxicity in larval zebrafish (*Danio rerio*), Sci. Total Environ. 882 (2023) 163595.
[17] W. Peng, C. Liu, D. Chen, et al., Exposure to N-(1,3-dimethylbutyl)-N′-phenyl-p-phenylenediamine (6PPD) affects the growth and development of zebrafish embryos/larvae, Ecotoxicology 232 (2022) 113221.
[18] K. Yao, Q. Kang, W. Liu, et al., Chronic exposure to tire rubber-derived contaminant 6PPD-quinone impairs sperm quality and induces the damage of reproductive capacity in male mice, J. Hazard. Mater. 470 (2024) 134165.
[19] L. Fang, C. Fang, S. Di, et al., Oral exposure to tire rubber-derived contaminant 6PPD and 6PPD-quinone induces hepatotoxicity in mice, Sci. Total Environ. 869 (2023) 161836.
[20] Z. Zhang, X. Xu, Z. Qian, et al., Association between 6PPD-quinone exposure and BMI, influenza, and diarrhea in children, Environ. Res. 247 (2024) 118201.
[21] X.L. Liao, Z.F. Chen, Q.Y. Liu, et al., Tissue accumulation and biotransformation of 6PPD-quinone in adult zebrafish and its effects on the intestinal microbial community, Environ. Sci. Technol. 58 (23) (2024) 10275–10286.
[22] T.Y. Choi, T.I. Choi, Y.R. Lee, et al., Zebrafish as an animal model for biomedical research, Exp. Mol. Med. 53 (3) (2021) 310–317.
[23] T. Tal, B. Yaghoobi, P.J. Lein, Translational toxicology in zebrafish, Curr. Opin. Toxicol. 23 (2020) 56–66.
[24] K. Hiki, K. Asahina, K. Kato, et al., Acute toxicity of a tire rubber-derived chemical, 6PPD quinone, to freshwater fish and crustacean species, Environ. Sci. Technol. Lett. 8 (9) (2021) 779–784.
[25] N. Grasse, B. Seiwert, R. Massei, et al., Uptake and biotransformation of the tire rubber-derived contaminants 6-PPD and 6-PPD quinone in the zebrafish embryo (*Danio rerio*), Environ. Sci. Technol. 57 (41) (2023) 15598–15607.
[26] B. Beliaeff, T. Burgeot, Integrated biomarker response: a useful tool for ecological risk assessment, Environ. Toxicol. Chem. 21 (6) (2002) 1316–1322.
[27] E. Guerlet, P. Vasseur, L. Giambérini, Spatial and temporal variations of biological responses to environmental pollution in the freshwater zebra mussel, Ecotoxicology 73 (6) (2010) 1170–1181.
[28] W. Guo, L. Lei, X. Shi, et al., Nonalcoholic fatty liver disease development in zebrafish upon exposure to bis(2-ethylhexyl)-2,3,4,5-tetrabromophthalate, a novel brominated flame retardant, Environ. Sci. Technol. 55 (10) (2021) 6926–6935.
[29] K.J. Livak, T.D. Schmittgen, Analysis of relative gene expression data using real-time quantitative PCR and the $2^{-\Delta\Delta CT}$ method, Methods 25 (4) (2001) 402–408.
[30] K. Wang, Y. Deng, J. Zhang, et al., Toxicity of thioacetamide and protective effects of quercetin in zebrafish (*Danio rerio*) larvae, Environ. Toxicol. 36 (10) (2021) 2062–2072.
[31] M. Huang, J. Jiao, J. Wang, et al., Characterization of acrylamide-induced oxidative stress and cardiovascular toxicity in zebrafish embryos, J. Hazard. Mater. 347 (2018) 451–460.
[32] B.R.M. Test, OECD guideline for the testing of chemicals, Mortality 1 (10) (1998).

[33] Q. Wang, J. Huang, S. Liu, et al., Aberrant hepatic lipid metabolism associated with gut microbiota dysbiosis triggers hepatotoxicity of novel PFOS alternatives in adult zebrafish, Environ. Int. 166 (2022) 107351.
[34] M. Li, M. Lv, T. Liu, et al., Lipid metabolic disorder induced by pyrethroids in nonalcoholic fatty liver disease of *Xenopus laevis*, Environ. Sci. Technol. 56 (12) (2022) 8463–8474.
[35] X. Zhang, Z. Peng, S. Hou, et al., Ubiquitous occurrence of p-Phenylenediamine (PPD) antioxidants and PPD-quinones in fresh atmospheric snow and their amplification effects on associated aqueous contamination, J. Hazard. Mater. 465 (2024) 133409.
[36] R. Jin, M. Venier, Q. Chen, et al., Amino antioxidants: a review of their environmental behavior, human exposure, and aquatic toxicity, Chemosphere 317 (2023) 137913.
[37] S. Di, H. Xu, Y. Yu, et al., Environmentally relevant concentrations of S-6PPD-quinone caused more serious hepatotoxicity than R-enantiomer and racemate in *Oncorhynchus mykiss*, Environ. Sci. Technol. 58 (40) (2024) 17617–17628.
[38] X.L. Liao, Z.F. Chen, S.P. Ou, et al., Neurological impairment is crucial for tire rubber-derived contaminant 6PPDQ-induced acute toxicity to rainbow trout, Sci. Bull. 69 (5) (2024) 621–635.
[39] D.E. Hinton, H. Segner, D.W. Au, et al., Liver toxicity, in: The Toxicology of Fishes, CRC Press, 2008, pp. 327–400.
[40] S. Sadekarpawar, P. Parikh, Gonadosomatic and hepatosomatic indices of freshwater fish Oreochromis mossambicus in response to a plant nutrient, World J. Zool. 8 (1) (2013) 110–118.
[41] L.C. Crowley, B.J. Marfell, N.J. Waterhouse, Analyzing cell death by nuclear staining with Hoechst 33342, Cold Spring Harb. Protoc. 2016 (9) (2016) pdb.prot087205.
[42] B.A. Neuschwander-Tetri, Non-alcoholic fatty liver disease, BMC Med. 15 (2017) 1–6.
[43] D. Maciejewska-Markiewicz, E. Stachowska, V. Hawryłkowicz, et al., The role of resolvins, protectins, and marensins in non-alcoholic fatty liver disease (NAFLD), Biomolecules 11 (7) (2021) 937.
[44] S.A. Parry, L. Hodson, Influence of dietary macronutrients on liver fat accumulation and metabolism, J. Investig. Med. 65 (8) (2017) 1102–1115.
[45] H. Guo, J. Wang, J. Yao, et al., Comparative hepatotoxicity of novel PFOA alternatives (perfluoropolyether carboxylic acids) on male mice, Environ. Sci. Technol. 53 (7) (2019) 3929–3937.
[46] D.J. Cuthbertson, E. Brown, J. Koskinen, et al., Longitudinal analysis of risk of non-alcoholic fatty liver disease in adulthood, Liver Int. 39 (6) (2019) 1147–1154.
[47] Y. Yan, D. Hou, X. Zhao, et al., Childhood adiposity and nonalcoholic fatty liver disease in adulthood, Pediatrics 139 (4) (2017).
[48] H. Jaeschke, Reactive oxygen and mechanisms of inflammatory liver injury: present concepts, J. Gastroenterol. Hepatol. 26 (2011) 173–179.
[49] N. Kaplowitz, Biochemical and cellular mechanisms of toxic liver injury, Semin. Liver Dis. 22 (2) (2002) 137–144. Thieme Medical Publishers, Inc.
[50] Z. Goc, W. Szaroma, E. Kapusta, et al., Protective effects of melatonin on the activity of SOD, CAT, GSH-Px and GSH content in organs of mice after administration of SNP, Chin. J. Physiol. 60 (1) (2017) 1–10.
[51] K. Erdoğan, Determination of acute toxicity of sodium pyrithione and its exposure effects on antioxidant enzymes activity, immune status, and histopathological changes in common carp, Chem. Ecol. 39 (4) (2023) 376–392.
[52] D. Tsikas, Assessment of lipid peroxidation by measuring malondialdehyde (MDA) and relatives in biological samples: analytical and biological challenges, Anal. Biochem. 524 (2017) 13–30.
[53] S. Gaweł, M. Wardas, E. Niedworok, et al., Malondialdehyde (MDA) as a lipid peroxidation marker, Wiad. Lek. 57 (9–10) (2004) 453–455.
[54] F.J. Romero, F. Bosch-Morell, M.J. Romero, et al., Lipid peroxidation products and antioxidants in human disease, Environ. Health Perspect. 106 (suppl 5) (1998) 1229–1234.
[55] K. Zoroufchi Benis, A. Behnami, S. Minaei, et al., Environmental occurrence and toxicity of 6PPD quinone, an emerging tire rubber-derived chemical: a review, Environ. Sci. Technol. Lett. 10 (10) (2023) 815–823.
[56] K. Anderson-Bain, C. Roberts, E. Kohlman, et al., Apical and mechanistic effects of 6PPD-quinone on different life-stages of the fathead minnow (*Pimephales promelas*), Comp. Biochem. Physiol. C Toxicol. Pharmacol. 271 (2023) 109697.
[57] X. Hua, G. Liang, J. Chao, et al., Exposure to 6-PPD quinone causes damage on mitochondrial complex I/II associated with lifespan reduction in Caenorhabditis elegans, J. Hazard. Mater. 472 (2024) 134598.
[58] J. Liu, M. Yu, R. Shi, et al., Comparative toxic effect of tire wear particle-derived compounds 6PPD and 6PPD-quinone to Chlorella vulgaris, Sci. Total Environ. 951 (2024) 175592.
[59] M. Amemiya-Kudo, H. Shimano, A.H. Hasty, et al., Transcriptional activities of nuclear SREBP-1a, -1c, and -2 to different target promoters of lipogenic and cholesterogenic genes, J. Lipid Res. 43 (8) (2002) 1220–1235.
[60] D. Fraher, A. Sanigorski, N.A. Mellett, et al., Zebrafish embryonic lipidomic analysis reveals that the yolk cell is metabolically active in processing lipid, Cell Rep. 14 (6) (2016) 1317–1329.
[61] K. Begriche, J. Massart, M.A. Robin, et al., Mitochondrial adaptations and dysfunctions in nonalcoholic fatty liver disease, Hepatology 58 (4) (2013) 1497–1507.
[62] S.Y. Bu, D.G. Mashek, Hepatic long-chain acyl-CoA synthetase 5 mediates fatty acid channeling between anabolic and catabolic pathways, J. Lipid Res. 51 (11) (2010) 3270–3280.
[63] S. Rong, V.A. Cortés, S. Rashid, et al., Expression of SREBP-1c requires SREBP-2-mediated generation of a sterol ligand for LXR in livers of mice, Elife 6 (2017) e25015.
[64] J.D. Horton, J.L. Goldstein, M.S. Brown, SREBPs: activators of the complete program of cholesterol and fatty acid synthesis in the liver, J. Clin. Investig. 109 (9) (2002) 1125–1131.
[65] S. Karanth, E.M. Denovan-Wright, C. Thisse, et al., The evolutionary relationship between the duplicated copies of the zebrafish fabp11 gene and the tetrapod FABP4, FABP5, FABP8, and FABP9 genes, FEBS J. 275 (12) (2008) 3031–3040.
[66] C.H. Li, X.M. Ren, L.H. Guo, Adipogenic activity of oligomeric hexafluoropropylene oxide (perfluorooctanoic acid alternative) through peroxisome proliferator-activated receptor γ pathway, Environ. Sci. Technol. 53 (6) (2019) 3287–3295.
[67] E.B. Mardian, R.M. Bradley, J.J.A. Henao, et al., Agpat4/Lpaatδ deficiency highlights the molecular heterogeneity of epididymal and perirenal white adipose depots, J. Lipid Res. 58 (10) (2017) 2037–2050.
[68] Y. Yang, T. Yang, Z. Zhao, et al., Down-regulation of BMAL1 by MiR-494-3p promotes hepatocellular carcinoma growth and metastasis by increasing GPAM-mediated lipid biosynthesis, Int. J. Biol. Sci. 18 (16) (2022) 6129.
[69] A. De Jesus, F. Keyhani-Nejad, C.M. Pusec, et al., Hexokinase 1 cellular localization regulates the metabolic fate of glucose, Mol. Cell. 82 (7) (2022) 1261, 77.e9.
[70] R. Banerji, C. Huynh, F. Figueroa, et al., Enhancing glucose metabolism via gluconeogenesis is therapeutic in a zebrafish model of Dravet syndrome, Brain Commun 3 (1) (2021) fcab004.
[71] H. Yang, K. Ou-Yang, Y. He, et al., Nitrite induces hepatic glucose and lipid metabolism disorders in zebrafish through mitochondrial dysfunction and ERs response, Aquat. Toxicol. 273 (2024) 107015.
[72] B.C. Zhang, J.H. Chen, C.H. Xiang, et al., Increased serum bile acid level is associated with high-risk coronary artery plaques in an asymptomatic population detected by coronary computed tomography angiography, J. Thorac. Dis. 11 (12) (2019) 5063.
[73] C.A. Flannery, G.H. Choe, K.M. Cooke, et al., Insulin regulates glycogen synthesis in human endometrial glands through increased GYS2, J. Clin. Endocrinol. Metab. 103 (8) (2018) 2843–2850.
[74] F. Long, M.R. Bhatti, A. Kellenberger, et al., A low-carbohydrate diet induces hepatic insulin resistance and metabolic associated fatty liver disease in mice, Mol. Metab. 69 (2023) 101675.
[75] M.N. Trinh, M.S. Brown, J. Seemann, et al., Interplay between Asters/GRAMD1s and phosphatidylserine in intermembrane transport of LDL cholesterol, Proc. Natl. Acad. Sci. 119 (2) (2022) e2120411119.
[76] P. Chen, L. Yao, M. Yuan, et al., Mitochondrial dysfunction: a promising therapeutic target for liver diseases, Genes Dis 11 (3) (2024) 101115.
[77] A. Mansouri, C.-H. Gattolliat, T. Asselah, Mitochondrial dysfunction and signaling in chronic liver diseases, Gastroenterology 155 (3) (2018) 629–647.
[78] C.E. Kosmas, I. Martinez, A. Sourlas, et al., High-density lipoprotein (HDL) functionality and its relevance to atherosclerotic cardiovascular disease, Drugs Context 7 (2018).
[79] D.Q. Sun, W.Y. Liu, S.J. Wu, et al., Increased levels of low-density lipoprotein cholesterol within the normal range as a risk factor for nonalcoholic fatty liver disease, Oncotarget 7 (5) (2016) 5728.
[80] P. Drapeau, L. Saint-Amant, R.R. Buss, et al., Development of the locomotor network in zebrafish, Prog. Neurobiol. 68 (2) (2002) 85–111.
[81] F. Seebacher, I. Walter, Differences in locomotor performance between individuals: importance of parvalbumin, calcium handling and metabolism, J. Exp. Biol. 215 (4) (2012) 663–670.
[82] A. Dutta, D.K. Sinha, Zebrafish lipid droplets regulate embryonic ATP homeostasis to power early development, Open Biol. 7 (7) (2017) 170063.
[83] A. Golla, H. Østby, F. Kermen, Chronic unpredictable stress induces anxiety-like behaviors in young zebrafish, Sci. Rep. 10 (1) (2020) 10339.
[84] G. Patki, N. Solanki, F. Atrooz, et al., Depression, anxiety-like behavior and memory impairment are associated with increased oxidative stress and inflammation in a rat model of social stress, Brain Res. 1539 (2013) 73–86.
[85] O.I. Rudko, A.V. Tretiakov, E.A. Naumova, et al., Role of PPARs in progression of anxiety: literature analysis and signaling pathways reconstruction, PPAR Res. 2020 (2020) 8859017.
[86] F. Beheshti, M. Hosseini, M. Hashemzehi, et al., The effects of PPAR-γ agonist pioglitazone on anxiety and depression-like behaviors in lipopolysaccharide injected rats, Toxin Rev. 40 (4) (2021) 1223–1232.
[87] P. Morigny, J. Boucher, P. Arner, et al., Lipid and glucose metabolism in white adipocytes: pathways, dysfunction and therapeutics, Nat. Rev. Endocrinol. 17 (5) (2021) 276–295.
[88] F.N. Varra, M. Varras, V.K. Varra, et al., Molecular and pathophysiological relationship between obesity and chronic inflammation in the manifestation of metabolic dysfunctions and their inflammation-mediating treatment options, Mol. Med. Rep. 29 (6) (2024) 95.
[89] Y.S. Lee, J. Olefsky, Chronic tissue inflammation and metabolic disease, Genes Dev. 35 (5–6) (2021) 307–328.
[90] B. Grygiel-Górniak, Peroxisome proliferator-activated receptors and their ligands: nutritional and clinical implications-a review, Nutr. J. 13 (2014) 1–10.
[91] H. Chen, H. Tan, J. Wan, et al., PPAR-γ signaling in nonalcoholic fatty liver disease: Pathogenesis and therapeutic targets, Pharmacol. Ther. 245 (2023) 108391.
[92] E.M. Brunt, V.W.S. Wong, V. Nobili, et al., Nonalcoholic fatty liver disease, Nat. Rev. Dis. Primers 1 (1) (2015) 1–22.

[93] H. Guterres, W. Im, Improving protein-ligand docking results with high-throughput molecular dynamics simulations, J. Chem. Inf. Model. 60 (4) (2020) 2189–2198.
[94] W. Lin, Y. Yan, S. Ping, et al., Metformin-induced epigenetic toxicity in zebrafish: experimental and molecular dynamics simulation studies, Environ. Sci. Technol. 55 (3) (2020) 1672–1681.
[95] B. Li, J. Chen, M. Long, Measuring binding kinetics of surface-bound molecules using the surface plasmon resonance technique, Anal. Biochem. 377 (2) (2008) 195–201.
[96] W. Ma, L. Yang, L. He, Overview of the detection methods for equilibrium dissociation constant KD of drug-receptor interaction, J. Pharm. Anal. 8 (3) (2018) 147–152.